Balancing the effect of corona on therapeutic efficacy and macrophage uptake of lipid nanocapsules

Sanchez-Moreno, P.; Buzon, P.; Boulaiz, H.; Peula-Garcia, J. M.; Ortega-Vinuesa, J. L.; Luque, I.; Salvati, A.; Marchal, J. A.

Published in:
Biomaterials

DOI:
10.1016/j.biomaterials.2015.04.049

Publication date:
2015

Biomaterials 61 (2015) 266–278

Contents lists available at ScienceDirect

Biomaterials

journal homepage: www.elsevier.com/locate/biomaterials

Balancing the effect of corona on therapeutic efficacy and macrophage uptake of lipid nanocapsules

P. Sánchez-Moreno [a, f, *], P. Buzón [c], H. Boulaiz [b, g], J.M. Peula-García [a, d], J.L. Ortega-Vinuesa [a], I. Luque [c], A. Salvati [e], J.A. Marchal [b, g, **]

[a] Biocolloid and Fluid Physics Group, Department of Applied Physics, University of Granada, 18071 Granada, Spain
[b] Biopathology and Regenerative Medicine Institute (IBIMER), Centre for Biomedical Research, University of Granada, Granada E-18100, Spain
[c] Department of Physical Chemistry, University of Granada, 18071 Granada, Spain
[d] Department of Applied Physics II, University of Málaga, 29071 Málaga, Spain
[e] Faculty of Mathematics and Natural Sciences, Pharmacokinetics, Toxicology and Targeting — Groningen Research Institute of Pharmacy, Antonius Deusinglaan 1, 9713 AV Groningen, The Netherlands
[f] European Center for Nanomedicine (CEN), Laboratory of Nanostructured Fluorinated Materials (NFMLab), Department of Chemistry, Materials, and Chemical Engineering "Giulio Natta", Politecnico di Milano, 20131, Italy
[g] Department of Human Anatomy and Embriology, Biosanitary Institute of Granada (ibs. GRANADA), University Hospitals of Granada-University of Granada, 18012 Granada, Spain

ARTICLE INFO

Article history:
Received 4 February 2015
Received in revised form
23 April 2015
Accepted 30 April 2015
Available online 13 May 2015

Keywords:
Lipid nanocapsules
Poloxamer
Protein corona
ITC
Docetaxel
Cancer

ABSTRACT

Several studies have shown the potential of biocompatible lipid nanocapsules as hydrophobic drug delivery systems. Understanding the factors that determine the interactions of these oil-in-water nanoemulsions with cells is a necessary step to guide the design of the most effective formulations. The aim of this study was to probe the ability of two surfactants with a markedly different nature, a non-ionic poloxamer, and a charged phospholipid, to prepare formulations with shells of different composition and different surface properties. Thus we determined their effects on the interaction with biological environments. In particular, we investigated how the shell formulation affected the adsorption of biomolecules from the surrounding biological fluids on the nanocapsule surface (corona formation). A complete physicochemical characterization including an isothermal titration calorimetry (ITC) study revealed that the use of poloxamer led to nanocapsules with a marked reduction in the number of protein-binding sites. Surface hydrophilicity and changes in corona formation strongly correlated to changes in uptake by cancer cells and by macrophages. Our results indicate that the nature and concentration of surfactants in the nanocapsules can be easily manipulated to effectively modulate their surface architecture with the aim of controlling the environmental interactions, thus optimizing functionality for *in vivo* applications. In particular, addition of surfactants that reduce protein binding can modulate nanoparticle clearance by the immune system, but also screens the desired interactions with cells, leading to lower uptake, thus lower therapeutic efficacy. The two effects need to be balanced in order to obtain successful formulations.

1. Introduction

The rapid advancement of nanomedicine has promoted the development of numerous nanosystems that can deliver drugs and other therapeutic agents to target tissues and that often possess complex structures and surface functionalizations [1–3].

Oil-in-water nanoemulsions, also known as lipid nanocapsules, have been studied in the pharmaceutical and medical fields because they show promise as drug carriers for their controlled and sustained release properties, subcellular size, inexpensive and

* Corresponding author. European Center for Nanomedicine (CEN), Laboratory of Nanostructured Fluorinated Materials (NFMLab), Department of Chemistry, Materials, and Chemical Engineering "Giulio Natta", Politecnico di Milano, 20131, Italy.
** Corresponding author. Department of Human Anatomy and Embriology, Biosanitary Institute of Granada (ibs. GRANADA), University Hospitals of Granada-University of Granada, 18012 Granada, Spain.
E-mail addresses: paola.sanchez@polimi.it (P. Sánchez-Moreno), jmarchal@ugr.es (J.A. Marchal).

http://dx.doi.org/10.1016/j.biomaterials.2015.04.049
0142-9612/

easy-to-scale production, independence of dilution, and biocompatibility [4]. Generally, these lipid nanocapsules consist of a hydrophobic inner core which can incorporate lipophilic drugs, and a hydrophilic outer shell that provides stabilization and offers the possibility of chemical modifications, among other important properties [5]. Lipid nanocapsules have become increasingly important for drug delivery in the field of cancer treatment, showing greater advantages over other lipid-based nanosystems in terms of leakage and drug loading [6], and they have been shown to be effective carriers for delivering hydrophobic drugs such as docetaxel [7–9]. Due to their nanoscale size, they can accumulate in tumor tissues more than in surrounding healthy tissue through enhanced permeability and retention effect (EPR) [10], and they can also be engineered and actively targeted with different molecules against overexpressed receptors of cancer cells [11–13].

Following intravenous administration, a nanoparticle is exposed to an evolved combinatorial system containing thousands of different proteins alongside lipids and sugars which can reconfigure nanoparticle dispersion and surface characteristics, forming a "corona" [14–19]. Recently, it has been shown that a biofunctional nanoparticle, quite basic in design, while showing specific recognition of biological receptors under model *in vitro* conditions, can lose uptake and receptor specificity as the complexity of the environment is increased by introducing human plasma [20]. The proteins adsorbed onto the original nanoparticle surface can mask targeting ligands and furthermore can interact with specific plasma membrane receptors on monocytes and various subsets of tissue macrophages, promoting rapid recognition and removal of the intravenously injected nanoparticles. Therefore, pharmacokinetics and biodistribution of nanoparticles are to a large extent governed by their surface properties, which in turn depend on the shell composition [21] and can be strongly altered upon interactions with complex biological environments [22].

To prolong their half life in the bloodstream by means of avoiding recognition by the mononuclear phagocyte system (MPS), different grafting materials have been tailored in drug delivery systems by using a variety of polymers such as poly (ethylene glycol) (PEG) and triblock copolymers (poloxamers and poloxamines). PEG is a flexible, electrically neutral, and hydrophilic polymer that has been commonly used to coat nanoparticles, to decrease the interaction of the surface with serum components, and to prolong particle circulation [23–26]. Poloxamers (Pluronic®) and poloxamines (Tetronic®) have been used for the same purpose with different levels of success [27–30]. They are amphiphilic nonionic block polymers composed by hydrophobic propylene oxide (PO) fragments and hydrophilic ethylene oxide (EO) branches. Poloxamers consist of a central poly-propylene oxide (PPO) backbone that is adsorbed onto hydrophobic interfaces, which is flanked on both sides by two hydrophilic chains of polyethylene oxide (PEO) that remain extended in the hydrophilic phase, yielding structures of the (PEO)a-(PPO)b-(POE)a type [31]. Another important property presented by poloxamer and poloxamines is the inhibition of multidrug resistance [32,33]. Most applications of triblock copolymers are based on their spontaneous self-assembly, leading to structures with a hydrophobic core (PPO) and a hydrophilic shell (PEO) [34,35], which however still present problems of low stability and degradation. Thus, an emerging application of poloxamers is their use as protective coating for nanocarriers (such as the oil-in-water nanoemulsions presented here), with the central POP block anchored onto the surface of the particles via hydrophobic interactions [36]. However further knowledge concerning the characteristics of pluronics as emulsifiers as well as their interactions with physiological media is needed to provide their rational use in the design of lipid nanocapsules.

Within this scenario the goal of the present study was to synthesize and physicochemically characterize lipid nanocapsule systems with different coatings, in order to study how the surface physicochemical properties of these colloidal particles influence protein adsorption, macrophage association, and uptake by cancer cells. Thus, four lipid core-shell nanosystems have been designed using a simple synthesis process. In all cases the hydrophobic core was constituted by olive oil, while the hydrophilic shell had a different composition. The commercially available and biocompatible surfactants composing the shell were Pluronic F127, also known as poloxamer 407, which has been chosen mainly because of its properties of long-term circulation [37], and Epikuron 145V (a mixture of phospholipid molecules), which provides a negative charge to the nanocapsule surface.

Isothermal titration calorimetry (ITC) is a known method to characterize the thermodynamic parameters of interactions between molecules in solution, but only more recently a few publications have described the use of ITC to study the binding thermodynamics of nanoparticles with proteins [38–41]. In the present study, ITC has been used to assess the binding thermodynamics of proteins onto the shells of the different lipid nanosystems developed. For this purpose binding studies have been performed using both a simplified model solution of bovine serum albumin (BSA) and a more complex biological fluid containing fetal bovine serum (FBS), to mimic the biological environment to which these nanocapsules are exposed. This allows to study in detail how addition of poloxamer into the formulation controls corona formation, thus also affecting nanoparticle uptake and therapeutic efficacy.

An uptake study in the human macrophage-like U937 cell line was also performed to determine the resistance of these nanocapsules to clearance by these cells depending on their surface composition. For these studies, coumarin 6 was encapsulated in the hydrophobic core of the nanocapsules and experiments were performed both under serum-free (SF) conditions as well as in the presence of serum (complete medium) (cDMEM); also, docetaxel-loaded nanosystems were prepared to perform a cytotoxicity assay in the A549 human lung cancer cell line.

Overall, the approach presented here, where physico-chemical characterization of the different nanocapsules in biological fluids is combined with the assessment of uptake and efficacy in relevant cell systems, allows us to explore how different formulations are processed by cells and the role of the different components in these interactions.

2. Results and discussion

2.1. Physico-chemical characterization of nanocapsules

2.1.1. Particle size

The synthesized nanoemulsions were stable under storage conditions —pure water and 4°C— for at least 3 months. The average diameter and PDI of the nanocapsules (see Fig. 1) were, respectively, 158 ± 5 nm and 0.108 for nanocapsules exclusively composed by lecithin (EP nanocapsules), 163 ± 3 nm and 0.110 for ME nanocapsules composed by a mixture of lecithin and poloxamer with a predominance of the first one, 215 ± 29 nm and 0.125 for nanocapsules with both surfactants with a predominance of poloxamer (MP nanocapsules), and 232 ± 29 nm and 0.146 for PL nanocapsules, exclusively composed by poloxamer. Thus, the hydrodynamic size of all the nanocapsule systems showed a narrow distribution (PDI < 0.15). Moreover these diameters are optimal for the use of these nanocapsules in potential *in vivo* applications allowing these drug delivery systems to extravasate into tumor tissues, accumulate, and release the therapeutic drug locally

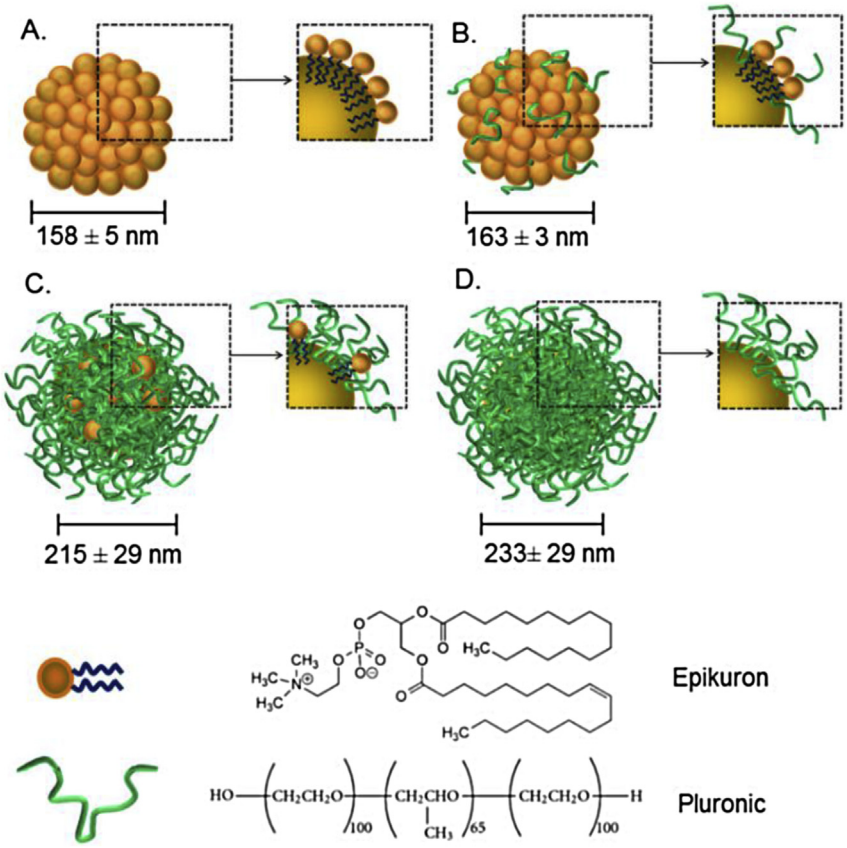

Fig. 1. Schematic details of the composition and size of the four different nanosystems. A) EP nanocapsules. B) ME nanocapsules. C) MP nanocapsules. D) PL nanocapsules.

through the "enhanced permeability and retention" (EPR) effect [42]. Given the size differences among the systems, Epikuron 145V appeared to be the best emulsifier, since the mean diameter was lower in the EP case when this molecule acted by itself to stabilize the formulation, and even when it was mixed with Pluronic F127 but remaining as the main component of the system (ME nanocapsules). When both types of molecules, i.e. Epikuron 145V and Pluronic F127, were mixed with poloxamer, which was the main component of the shell, and when the poloxamer acted by itself to stabilize the emulsion, the nanocapsules size increased. These results agree with previous data in which the presence of poloxamer together with lecithin increased the particle size in comparison to the case in which lecithin was the only shell component [43].

2.1.2. Electrophoretic mobility

The electric state of the different nanoparticles was determined by electrophoretic mobility (μe) measurements. This experimental parameter is directly related to the zeta potential in the shear plane of the particles and is typically used to obtain information about the surface electrical state of colloidal systems and the composition of the nanocapsule surfaces [44,45]. This parameter is also influenced by both the ionic strength as well as the pH of the dispersion medium. In our case, the weak acid character of surface charged groups from the shell formed by Epikuron 145V was revealed by the pH titration curve of μe, with zeta potential constant values around −65 mV at neutral and basic pH (see Fig. 1 in Ref. [46]. However, the most relevant result is related when Pluronic F127 was gradually added in the different formulations. The main effect when these non-ionic surfactant molecules were present in the nanocapsule surfaces was the μe and zeta potential reduction (in absolute value) in comparison with the pure Epikuron 145V nanocapsules (EP), since the presence of polyethylene oxide (PEO) chains caused a displacement of the shear plane of the diffuse layer, resulting in lower electrokinetic charge values [47,48]. This was the case of ME nanocapsules, in which the zeta potential decreases up to − 41.6 mV at neutral pH, and also the MP nanocapsules (with even lower value, −19,2 mV, by increasing the pluronic concentration and decreasing the epikuron load). Finally, PL nanoparticles with a shell constituted only by Pluronic F127 presented the lowest zeta potential value (neutral or nearly neutral). It is evident that mobility, and consequently zeta potential, come from a combination of electrical and frictional forces and the presence of this non-ionic surfactant on the particles affects both forces [43,49].

The ability of the poloxamer molecules to alter the protein adsorption on lipid nanoparticles was studied by incubating the entire system in 10% of fetal bovine serum at 37 °C. The presence of protein molecules adsorbed onto the particles could be determined by studying the electric state of the different nanoparticles, since usually, the isoelectric point (IEP) of such complexes is determined by the degree of protein coverage, gradually tending to the pure protein IEP when the protein load on the nanoparticles surface increases [50,51]. Therefore, a clear correlation has been found between the mobility data and the amount of surface protein [52].

The μe data after FBS incubation reflected the presence of proteins adsorbed onto the nanocapsule surfaces modifying their original surface charge density. Moreover, clear differences appeared depending on the nature of the nanocapsule shell as a consequence of the different degree of protein coverage (Fig. 2). For EP nanocapsules, the electrophoretic mobility even inverted its sign at pH 4 where protein molecules of the FBS are positively charged, showing the highest variation from −4.14 to 0.64, nearly five mobility units. Protein adsorption on nanoparticles having a

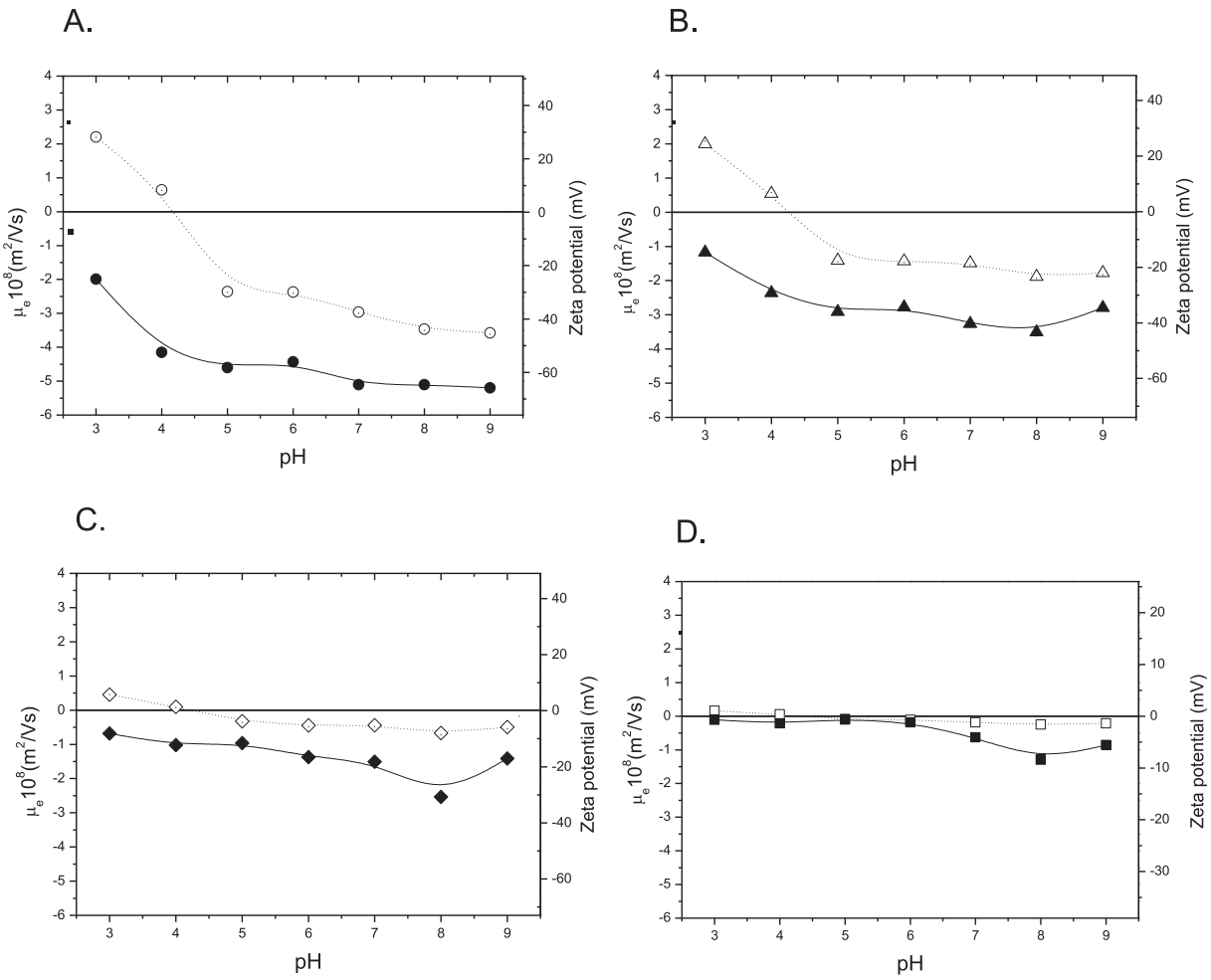

Fig. 2. Bare nanocapsules and nanocapsules incubated with 10% FBS for 1 h at 37 °C, A) EP (○, ●), B) ME (△, ▲), C) MP (◇, ◆) and D) PL (□, ■) nanoparticles. Dashed lines with solid symbols correspond to particles after the exposure with proteins, while solid lines with blank symbols refer to the bare nanoparticles.

combination of both surfactants, epikuron and pluronic, at their surfaces also resulted in changes in the surface charge of the nanocapsules: at pH 4 the μe values changed from −2.36 to 0.54 for the ME nanocapsules, and from −1.01 to 0.10 for the MP nanocapsules. An inverse relationship was found between the concentration of poloxamer in the shell and the μe shift after FBS incubation, indicating that the presence of poloxamer in the interface of the nanocapsules reduced protein adsorption, a result that agrees with several other studies [53,49,54]. In the same line, analyzing the μe values at neutral and basic pH, we found a similar relation between the μe decreasing (in absolute value) and the poloxamer amount in the nanocapsule surfaces, which is translated into a lower quantitative reduction of the original negative surface electrostatic potential when the poloxamer amount increases. In this manner, the lowest difference was found in the entire pH range when the PL nanoparticles were compared before and after the FBS incubation, which is indicative of a lesser extent of protein adsorption in this type of particle. In particular, at pH 4 the electrophoretic mobility barely changed. Roser et al. showed that neutrally charged particles have a much lower opsonization rate than do charged particles, demonstrating a direct correlation between surface charge and protein binding [55]. Therefore, the use of molecules such as poloxamers which can hinder the electrostatic and hydrophobic interactions is a good method to reduce unspecific protein adsorption.

2.1.3. Colloidal stability

The stability of the samples was studied at physiological pH (7.4) at different concentrations of two different electrolytes (NaCl and $CaCl_2$) by analyzing the change in the diameter of the particles as a function of time.

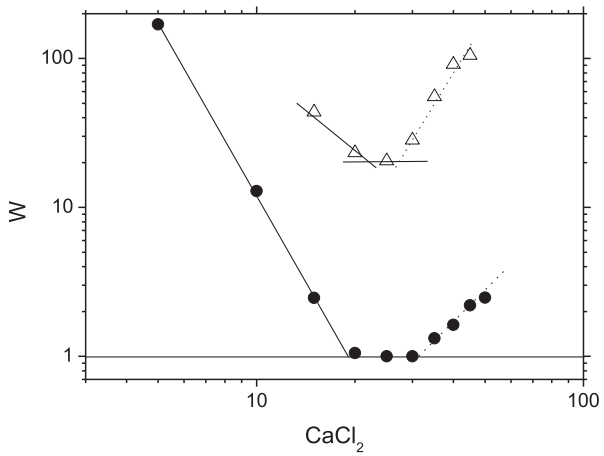

Fig. 3. Stability factor vs. calcium chloride concentration at pH 7.4: EP nanocapsules (●), and ME ones (△). The solid line helps to locate the CCC value, while dashed lines point to the CSC data.

The analysis of the coagulation kinetics of the nanosystems enables the calculation of the stability factor, W, and hence the critical coagulation concentration (CCC) and the critical stabilization concentration (CSC) of the nanoparticles. A deep explanation about how "W" is calculated, as well as the information that can be extracted from the CCC and CSC data is given in the supplementary section. Fig. 3 shows the stability factor vs. salt concentration. After the CCC and CSC values are analyzed, both the "effective surface charge" and the "hydrophilicity character of the surface" of our nanosystems can be estimated. We consider appropriate to remind in this point that both parameters are modulated by the presence of proteins on the surface if incubation in FBS took place. As expected, those CCC values with $CaCl_2$ were consistently lower than those with NaCl because divalent ions have a greater screening capacity, favoring the aggregation of the system. CSC values are dependent of the hydration forces that appear at medium and high ionic strengths on hydrophilic nanoparticles when great amounts of hydrated ions accumulate near the surface. The repulsive hydration forces begin to act, improving the stability of the nanosystem when the salinity value exceeds the CSC value [56,57]. Again, calcium showed higher restabilization capacity compared to sodium, since it is a more hydrated cation. With respect to the stability of the system in NaCl, no aggregation of the particles was detected even at concentrations up to 4 M because the CCC and CSC concentrations overlapped, inducing completely stable systems.

An analysis of the colloidal stability in $CaCl_2$ (see Table 1 and Fig. 3) indicated that EP nanocapsules were the least stable of the systems studied, presenting the lowest CCC value. The presence of poloxamer molecules adsorbed onto the shell of ME nanosystem was corroborated, as these particles are more stable than pure epikuron ones. No aggregation of MP or PL nanoparticles was detected because the concentration of poloxamer was higher on their shells and these molecules contribute to the stabilization of the systems by means of a steric mechanism and increase the surface hydrophilicity attributed to the PEO fragments. In comparison with standard characterization methods such as the determination of hydrodynamic size in different media [58,59,12] the study of the CCC and CSC (obtained from the aggregation kinetics of colloidal systems) allows to gain information about both the aggregation phenomena of the colloidal systems and also the surface characteristics of the particles. Those parameters cannot be obtained from the hydrodynamic size studies.

The presence of a protein corona after the incubation of the particles with 10% FBS can also be detected with these experiments because the colloidal stability is altered. On the one hand, proteins adsorbed onto a particle surface usually decrease the (absolute) charge of it, as observed above, reducing the electrostatic repulsive interactions among the particle surfaces predicted by the classical DLVO theory that accounts the stability of colloidal systems. On the other hand, however, the adsorbed protein layer can also provide an important additional stability by creating a steric hindrance based on structured water molecules, since this hydrophilic protein layer tends to be strongly hydrated [56,57]. This repulsive potential barrier comes from the so-called "hydration forces", and it is clearly reflected in restabilization processes when the ionic strength of the medium is increased.

These restabilization phenomena (that were previously shown in Fig. 4 working with our systems in absence of proteins), it clearly manifested after the exposure to proteins because all our nanosystems were completely stable in all the NaCl concentration range tested, even at very high salinity conditions.

The CCC and CSC values of ME nanoparticles were compared in calcium before and after the FBS incubation, and despite that in the first case they aggregated, after incubation they were stable at all

Table 1
Critical coagulation concentrations (CCC) and critical stabilization concentration (CSC) of our different nanocapsules before (bare nanoparticles) and after incubation with 10% FBS (nanoparticles + protein corona).

pH 7,4 $CaCl_2$	Bare nanoparticles		Nanoparticles + protein corona	
	CCC (mM)	CSC (mM)	CCC (mM)	CSC (mM)
EP	19	31	70	75
ME	22	25	stable	stable
MP	stable	stable	stable	stable
PL	stable	stable	stable	stable

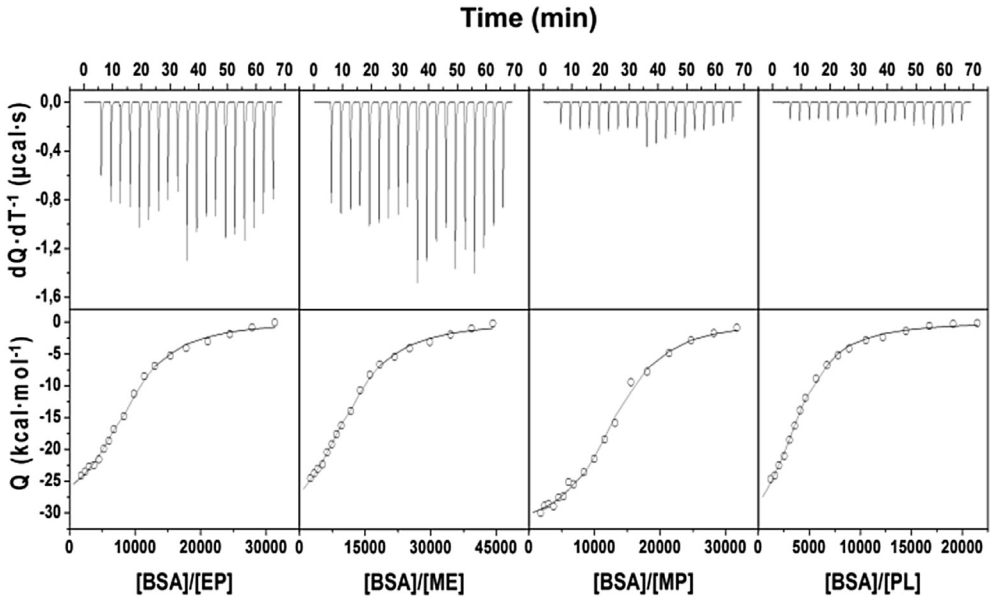

Fig. 4. Isothermal titration calorimetry experiments for EP, ME, MP, and PL nanoparticles with BSA at 25 °C in 2 mM sodium phosphate pH 7.4. Upper panels show the heat effects associated with the injection of BSA into the calorimetric cell containing the nanoparticles. Lower panels show the corresponding binding isotherm normalized for nanoparticle concentration and corrected for the heat of BSA dilution. Solid lines correspond to the best fit of data to a one-site model (Eq. (1)).

the $CaCl_2$ concentrations. This confirms the presence of proteins adsorbed onto the surface, as reflected in the electrophoretic mobility results. The EP nanocapsules also showed significant stability differences, revealing a different surface composition after the incubation with the FBS, due to the presence of a protein corona surrounding the original shell of the particles. From these experiments, no conclusions concerning the presence of a protein corona could be drawn about the MP and PL nanoparticles because their behavior was the same before and after the FBS incubation. Surface differences were not detected due to the complete stability they showed in all the cases.

2.2. Calorimetric study of protein adsorption

A combination of different techniques are necessary to provide a full picture of nanoparticle hard and soft protein corona and depending on the type of nanoparticles studied one of them are more suitable than others. An important methodological problem when studying the protein corona, is to separate free proteins from proteins bound to nanoparticles [60]. One of the preferred methods has been centrifugation, that has been applied with some success to identify the hard corona via other techniques such as mass spectrometry [61–63]. In the case of our nanocapsules, it is a perturbing method that cannot be used since the nanoparticles aggregate, and moreover minor particle-associated proteins are not identified by centrifugation. A method that permits the quantification of protein adsorption in situ, is fluorescence correlation spectroscopy (FCS) that determines binding affinities of proteins to nanoparticles and the thickness of the protein corona [17,64] The drawback of this technique is that FCS requires either fluorescently labeled nanoparticles or labeled proteins.

In this study isothermal titration calorimetry was selected as a method to further investigate the differential protein adsorption potential of the different nanosystems. ITC provides a full thermodynamic characterization of the binding equilibrium in terms of binding affinity, number of binding sites and enthalpic and entropic contribution to the Gibbs energy of binding, reporting on the nature and magnitude of the forces driving the protein-surface interaction. Upper panels in Fig. 4 show the calorimetric titrations of the four types of nanocapsules with BSA. The corresponding binding isotherms are shown in the lower panels together with the best fit to a one-set-of-sites model. The results of the thermodynamic analysis are summarized in Table 2.

BSA bound to nanocapsules with moderate dissociation constants in the low micromolar range. In all cases, protein binding was driven by a strongly favorable binding enthalpy that increased progressively with poloxamer content resulting in differences in binding enthalpy up to 5 kcal mol^{-1} between EP and PL nanocapsules. This increment in binding enthalpy was partially compensated for by a parallel increase in unfavorable entropic contributions for poloxamer containing nanocapsules, that could be partially associated to the reduction in the conformational degrees of freedom of the longer poloxamer side chains. These two opposing contributions result in a slight increase (of about 1 kcal mol^{-1}) in binding affinity for MP and PL particles with respect to ME and EP. Most notably, high poloxamer content led to a marked reduction in the number of binding sites (n/Area in Table 2) that dropped from 116×10^3 sites per μm^{-2} for the EP particles to 24×10^3 sites per μm^{-2} for the PL particles.

A similar set of titration experiments were performed with FBS in order to validate the results found with isolated BSA. As above, the binding properties of the nanocapsules changed progressively as they were enriched with poloxamer. Interestingly, as illustrated in Fig. 5, titrations of EP and ME nanocapsules with FBS show more complex binding isotherms that cannot be described by a simple one-set-of-sites model but can be adequately reproduced by a model considering two different sets of sites. This analysis revealed a tight binding event, characterized by dissociation constants in the nanomolar range, superposed on another characterized by dissociation constant close to what was measured for the isolated BSA. This tight binding contribution was not observed for PL particles, since it was perfectly described by the one-set-of-sites model. In the case of MP particles, an intermediate behavior was observed. The curve could be fitted to a one-set of sites model, although slight systematic deviations were observed at high saturation.

For all particles, at least one binding event with binding affinities very close to those measured for BSA was identified. It has been observed that in complex fluids such as serum typical coronas are formed by two different layers: a first layer of molecules with very high affinity for the particle surface, known as hard corona, characterized by very high residence time on the nanoparticle, and a second layer of proteins more loosely associated to the nanoparticle and in rapid exchange with the environment, known as soft corona. Thus here the 2 binding events could reflect this, with the hard corona proteins showing dissociation constants in the nanomolar range, and soft corona proteins with dissociation constants in the micromolar range. This would also suggest that simplified protein solutions such as here BSA may associate poorly to the nanoparticles comparing to what is observed for some proteins in more complex protein mixtures. Furthermore, the results would also suggest that the proteins associated to PL capsules are not only less abundant, but also more loosely bound to the surface, in comparison to what observed for the other formulations in serum, thus addition of pluronic in the formulation seem to prevent formation of a tightly bound hard corona layer. According to the thermodynamic results, increasingly unfavorable entropic contributions are observed for FBS binding to pluronic particles; this probably being related to the high entropic cost of fixing the conformation of the

Table 2
Binding thermodynamics of BSA and FBS to nanocapsules (NCs). n: number of binding sites; Kd: Dissociation Constant; H: Enthalpy; T: Temperature; S: Entropy; G: Gibbs Free Energy. Thermodynamic parameters obtained considering a total protein concentration in FBS of 40 mg/mL and the BSA molecular weight.

	NCs	n (10^3)	n/Area (10^3 n·μm^{-2})	Kd (μM)	ΔH_{ap} (kcal·mol^{-1})	$-T\cdot\Delta S_{ap}$ (kcal·mol^{-1})	ΔG_{ap} (kcal·mol^{-1})
BSA	EP	9.1	116.0	4.7	−30.1	22.9	−7.2
	ME	11.8	141.4	7.2	−32.9	25.9	−7.0
	MP	13.0	89.5	1.1	−32.6	24.4	−8.2
	PL	4.1	24.0	1.0	−35.0	26.8	−8.2
FBS	EP	53.5	682.1	3.6	−3.0	−4.4	−7.4
		16.8	214.2	0.057	−11.4	1.5	−9.9
	ME	68.6	821.9	2.5	−1.9	−5.7	−7.6
		19.6	234.8	0.071	−11.7	1.9	−9.8
	MP	32.7	225.2	1.8	−11.1	3.2	−7.9
	PL	11.0	64.5	3.9	−18.4	11.0	−7.4

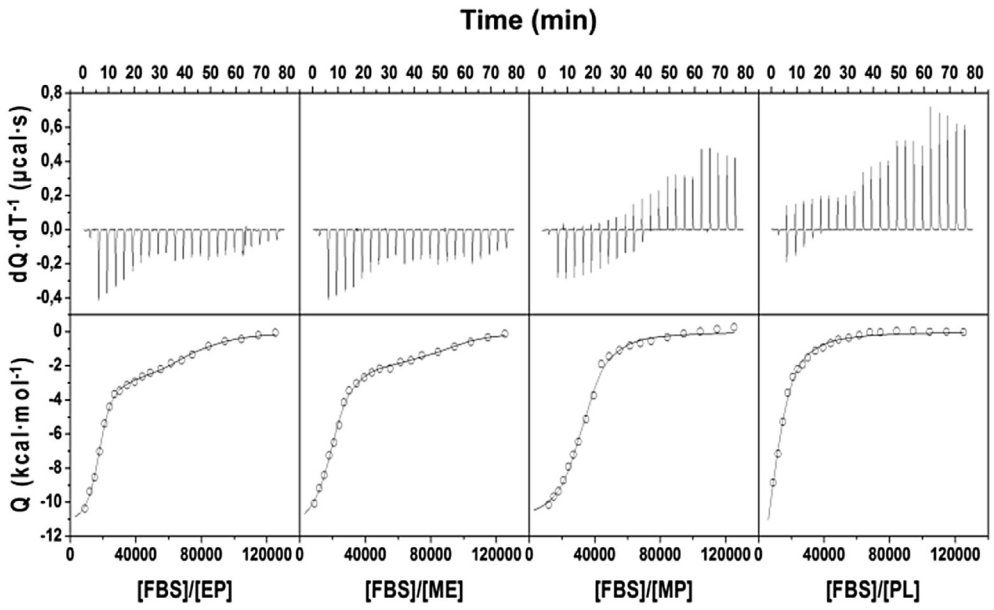

Fig. 5. Isothermal titration calorimetry experiments for EP, ME, MP and PL nanoparticles with FBS at 25 °C in 2 mM sodium phosphate pH 7.4. Upper panels show the heat effects associated with the injection of FBS into the calorimetric cell containing the nanoparticle. Lower panels show the corresponding binding isotherm normalized for nanoparticle concentration and corrected for the heat of FBS dilution. Solid lines correspond to the best fit of the data to a one-site model (Eq. (1)) in the experiments with MP and PL nanoparticles, and to a two sets of independent binding sites model (Eq. (2)) in the experiments with EP and ME nanoparticles.

long pluronic chains upon protein binding.

Because protein concentration cannot be determined exactly for FBS, the values for the number of binding sites calculated from these experiments cannot be quantitatively compared with those derived from the BSA titrations. Nonetheless, a similar trend was detected, with a significant reduction in the number of binding sites for MP particles that was even more pronounced for PL nanocapsules.

Taken together, all these results clearly indicate that an increase in the poloxamer content yields to a progressive modulation of the protein adsorption behavior of the nanocapsules, minimizing the protein binding capacity through a marked reduction in the number of binding sites. Furthermore, the (fewer) proteins bound on PL nanocapsules are characterized by a higher dissociation constant, suggesting that this coating allows reduction of hard corona formation.

2.3. *In vitro uptake of nanocapsules by cancer cells*

For an understanding of how the uptake of lipid nanocapsules by A549 human lung cancer cells is affected by the shell composition and the presence or absence of a preformed corona in serum, A549 cells, as a model of cancer cells, were exposed to our four types of nanocapsules in SF and cDMEM and their uptake was measured by flow cytometry. Coumarin 6, which has been extensively used as a fluorescent marker of lipid nanoparticles [65–67], was encapsulated in the core of the lipid nanosystems. A well known issue is that flow cytometry cannot distinguish between adhering and internalized particles and this has been studied in large detail [68,69]. To ensure that surface-adherent nanoparticles are removed, washing protocols, procedures for fixing the cells, and the optimal timing of all of these procedures have been optimized [70]. Moreover, it has been determined that after few hours of exposure, in most cases the amount of adhering particles is minimal in comparison to the active uptake and the internalized load [69]. Fig. 6 shows the results for cells treated for 3, 7, 24, and 48 h with the different nanoparticle systems dispersed in cDMEM.

When the uptake of the nanosystems was studied in cDMEM, significant variations among the nanocarriers with different shell composition were found. Thus for EP nanocapsules, at all the time points studied, the uptake was higher compare with the other nanocapsules. These particles constituted by a lecithin shell were taken up to a much greater extent than those with a high concentration of poloxamer in the shell.

The data reported showed that with increasing poloxamer concentration in the shell of the particles, the cellular uptake decreased. This was present early in the uptake profile, but the differences between particles increased with the exposure time. These results suggest that coatings which prevent protein binding may also make interactions with cells more difficult, thus leading to a lower uptake. In other words, addition of coatings such as PL does not only decrease interactions of the nanoparticles with the surrounding proteins, thus decreasing unspecific binding, but also can decrease interactions with the cell membrane and cell receptors,

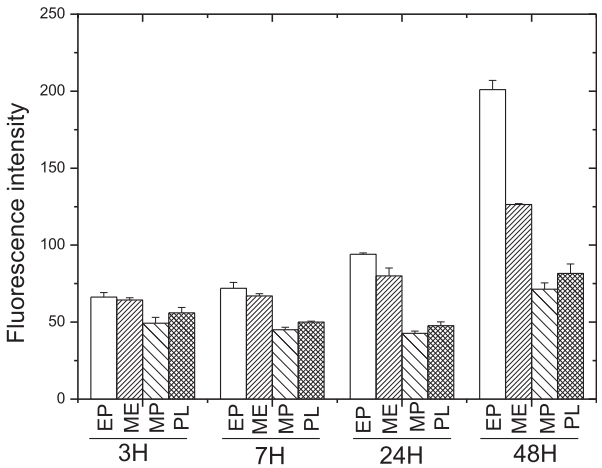

Fig. 6. Quantitative study of cellular uptake efficiency for the EP, ME, MP, and PL nanocapsules loaded by Coumarin 6 in A549 cells after 3, 7, 24, and 48 h.

leading to lower uptake by cells.

Clearly, ideal formulation should balance between these two effects or additional modifications should be included to ensure that the desired interactions with the target cell or receptors are achieved.

Surface hydrophobicity has been considered to be a major determinant of cellular response. This property can affect the interaction of the nanocapsules with the different components of the cell membrane, favoring not only the interaction between cells and nanoparticles, but also affecting the permeability of the membrane as a result of interactions with the bilayer phospholipids or other lipidic molecules as cholesterol whose activity is related to the fluidity and reorganization of the membrane and endocytosis processes [71]. On the other hand, the protein binding data from physicochemical characterization experiments suggest that an increase in the interface hydrophobicity will also result in an increase in protein adsorption. Because there is a large number of proteins on the cell surface, the interaction between the cell and nanocapsules becomes stronger, and the uptake by the cells is higher if the protein adsorption ability is strengthened. In fact, it has been demonstrated by Hu et al. that when polymeric nanoparticles are used against the HepG2 cell line, cells preferred to attach to more hydrophobic polymers [72]. Comparable results were observed by Allen et al. studying the cellular response to interaction with a series of copolymer films, determined by the surface adsorbed protein layer [73].

Higher uptake levels in SF were observed for all the four nanosystems investigated (see Fig. 2 of Ref [46]). This is in agreement with similar results in literature, where higher uptake was observed for particles exposed to cells in SF conditions [71]. It has been observed in fact that in the absence of corona, adhesion of the bare surface of the nanoparticles to cell membrane is much higher than when the nanoparticle surface is covered by a corona [72], leading to higher uptake into cells. The importance of hydrophobic lipid–lipid interactions in this situation was highlighted by Montis et al. [73] working with synthetic lipid membranes. These authors found a cell membrane restructuring which increased the permeability for nanoparticles without protein corona. In our case, this situation is favored in nanocapsules having the highest concentration of phospholipids at the interface, which produces a higher uptake versus nanocapsules with pluronic molecules. The uptake was studied for up to 24 h because after that time, cells exposed to several types of particles changed their phenotype and lost cell adhesion, which is indicative of cell damage, as also observed for other particles when exposed to cells in absence of corona [71], due to the strong adhesion of bare nanoparticle surfaces to the cell membrane. In fact, we could not determine the uptake by flow cytometry of EP nanoparticles in SF because they seriously damaged cells already after short exposure times. These results clearly confirm that the nature of interactions of the same material in the presence or absence of proteins differed. The trend for the four types of nanoparticles studied confirmed what observed in the cDMEM case, thus also in SF conditions, as the concentration of Pluronic F127 increased in the shell, uptake decreased.

Cellular uptake efficiency of nanoparticles by A549 cells was further evaluated qualitatively using fluorescence microscopy after 24 h of incubation (Fig. 7). The comparison of cells exposed to the different nanocarriers shows that the green fluorescence intensity in cells treated with EP nanoparticles is higher than in cells incubated with the other nanosystems, indicating higher cellular uptake efficiency in agreement with flow cytometry results. When the concentration of poloxamer increased on the surface of the carriers, the green fluorescence intensity surrounding DAPI-stained nuclei decreased, and hence the uptake efficiency. The staining of the cells incubated with nanoparticles composed mainly by Epikuron 145V (EP and ME nanocapsules) (Fig. 7b and c) was stronger than in those treated with free Coumarin 6 (Fig. 7f) and particles with a high concentration of Pluronic F127 (MP and PL nanocapsules) (Fig. 7d and e). No green fluorescence was detected either when cells were incubated with the four types of blank particles (data not shown) or in the untreated control sample (Fig. 7a), the images presenting only the blue fluorescence from the stained nuclei.

2.4. Cytotoxicity assays of docetaxel-loaded nanoparticles

The therapeutic effect of docetaxel-loaded nanocapsules (DOC-nanoparticles) was determined by sulforhodamine-B colorimetric assay on A549 cells. Cells were treated with increasing concentrations of free docetaxel or the different docetaxel-loaded nanocapsules for 48 h. The analysis of the encapsulation efficiency of docetaxel by high-performance liquid chromatography (HPLC) showed that during the first 5 h of dialysis some 80% of the docetaxel which was in the core of the particles was released due to their amphiphilic coating. From this time point up to 24 h, 20% of docetaxel remained encapsulated in the oily core (see Ref. [46] Fig. 4). Although the interface composition of the nanoparticles was different, they all behaved almost similarly in terms of leakage, maintaining a concentration of docetaxel therapeutically effective after the purification process. In order to study the therapeutic effect of internalized capsules without additional effects due to the release of docetaxel prior to uptake into cells, capsules were added to cells after 24 h dialysis.

Fig. 8 shows the inhibitory concentration 50 (IC_{50}) values determined in A549 cells after treatment with DOC-nanoparticles (see raw data in Fig. 5 of Ref. [46]). These cells were also treated with empty EP, ME, MP or PL nanoparticles and no significant differences in cell growth were found in comparison with untreated A549 cells (data not shown), signifying that empty nanocapsules were not toxic to cells at the concentrations used for the study. A first important observation is that cells treated with all the different formulations of docetaxel-loaded nanocapsules showed a markedly lower proliferation rate in A549 cells than those treated with free docetaxel. In fact, the four types of docetaxel-loaded nanoparticles induced high cell-death levels, exerting 11.1-fold (DOC-EP), 8.0-fold (DOC-ME) and 3.2-fold (DOC-MP and DOC-PL) more potent cytotoxic effect than did free docetaxel. These results indicate that the treatment with docetaxel-loaded nanocapsules enhanced drug internalization by A549 cells, allowing a substantial decrease in the dosage. A decrease in dosage, in an *in vivo* system, is mostly beneficial as it reduces side effects often observed when higher doses are administered.

These results were consistent with our previous findings after exposure of MCF 7 breast cancer cells to lipid nanocapsules composed of a different shell but similarly loaded with docetaxel [7]. According to the findings of Liu et al. the *in vitro* cytotoxicity of docetaxel-loaded micelles was lower than that of the conventional docetaxel formulation at 37 °C [74]. Therefore, the greater cytotoxicity reported here compares favorably with these results.

Furthermore, when analyzing efficacy of the different formulations, we could observe that DOC-MP and DOC-PL nanocapsules, characterized by a higher amount of Pluronic F127, showed lower cytotoxicity than did the particles with lower concentration of this molecule in the shell (DOC-ME nanoparticles) and the pure epikuron ones (EP nanoparticles).

Thus the most cytotoxic particles were those without Pluronic F127 (DOC-EP) and, as the concentration of poloxamer increased in the shell of the particles, the cytotoxicity decreased. This phenomenon appeared to correspond reasonably well to the cellular uptake efficiency, the protein adsorption, and the hydrophilicity character of the surfaces.

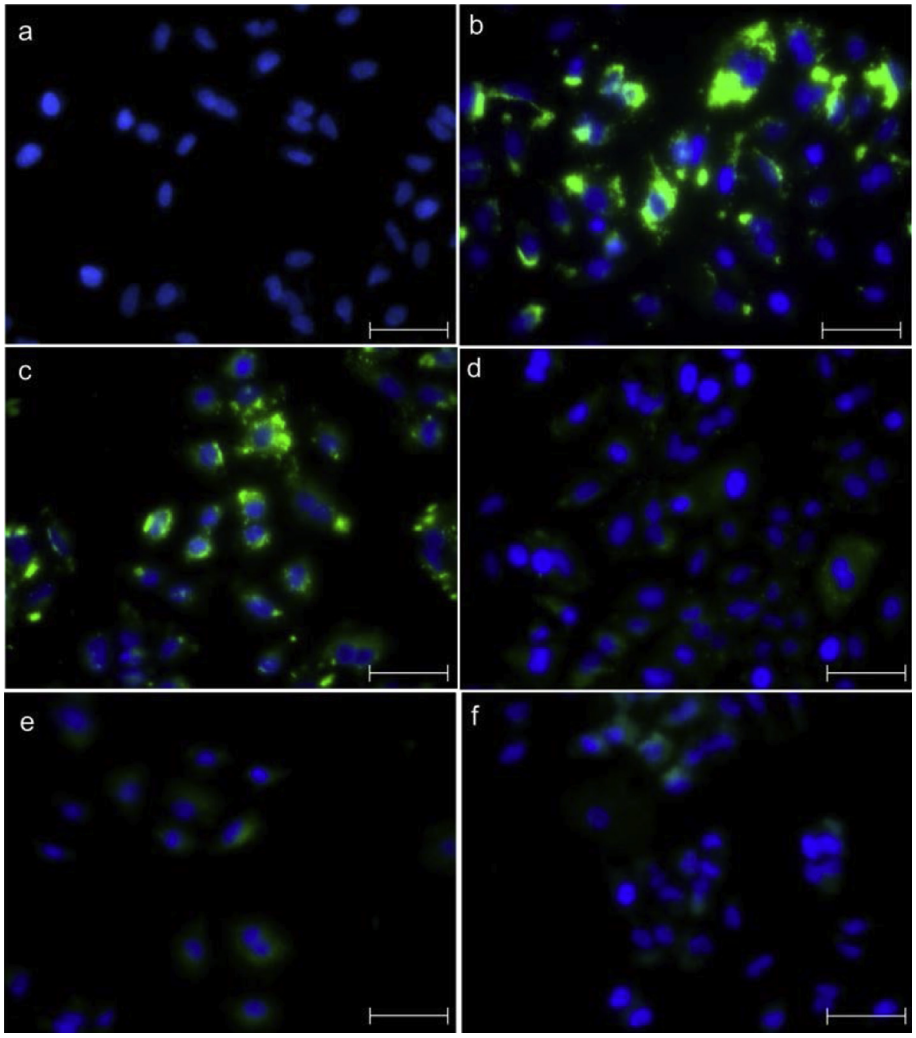

Fig. 7. Fluorescence microscopy of A549 cells (scale bar 50 μm) after incubation with free Coumarin 6 (f) and Coumarin 6 loaded EP (b), ME (c), MP (d), and PL (e) nanocapsules for 24 h. The control of untreated cells is also shown (a).

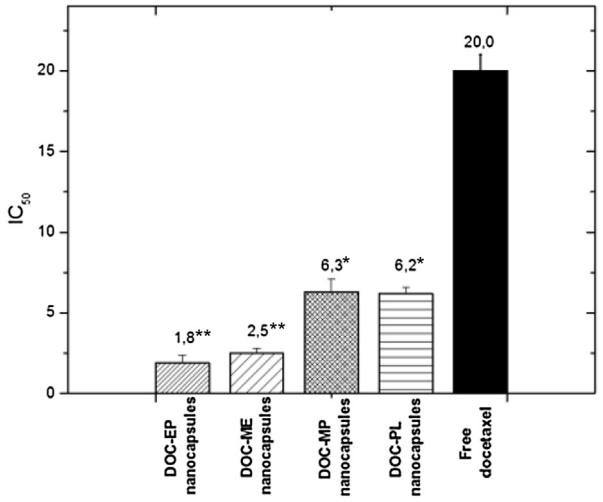

Fig. 8. IC_{50} values (drug concentration producing 50% reduction in absorbance in control cells) of free docetaxel and docetaxel-loaded nanoparticles, expressed in nM. Statistically significant **P < 0.01 vs control; *P < 0.05 vs control.

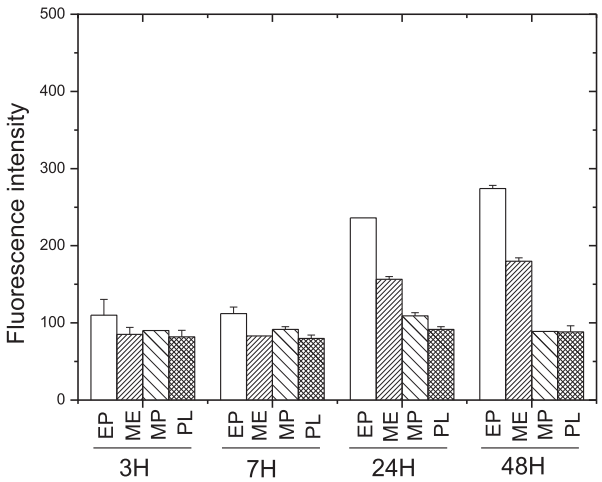

Fig. 9. Quantitative study of cellular uptake efficiency for the EP, ME, MP and PL nanocapsules loaded by Coumarin 6 in macrophage like activated U937 cells after 3, 7, 24, and 48 h.

2.5. In vitro uptake of nanocapsules by macrophages

In addition to the *in vitro* studies of the particles in A549 cells, an uptake assay was performed in the monocytic cell line U937 to determine how the macrophage uptake of these nanocapsules is affected by the shell composition. Fig. 9 presents the fluorescence intensity detected by flow cytometry after 3, 7, 24, and 48 h of exposure of macrophage-like activated U937 cells to our different nanosystems loaded with Coumarin 6 dispersed in cDMEM.

The trend of uptake in activated U937 cells was the same as the one observed in A549 cells. In both cases the uptake by cells was higher in EP nanosystems and this uptake was reduced when the concentration of poloxamer increased on the surface. In both cases the steric repulsion effect produced by the extended PEO chains of Pluronic F127 prevented protein adsorption and thus, interactions with macrophages and A549 cells. Different concentrations of Pluronic may also lead to different configurations of the polymer chains: in fact, PEG chains, which have the same structure as PEO chains of poloxamer, are known to form different structures on the surface of the particle at low or high surface coverage. At low concentration PEG chains adopt a configuration called "mushroom" where they are located closer to the surface, and can leave gap between the chains. At higher concentration of PEG and pluronic, instead, a different configuration known as "brush" is adopted, where the motion of the chains is restricted, guaranteeing a complete coverage of the surface [75,76]. Stolnik et al., working with polystyrene nanoparticles which were incubated with different concentrations of poloxamer, found a different percentage of surface coverage and showed a decrease in protein adsorption when the coverage by poloxamer was increased and this improved circulation time in blood [77]. Uptake by macrophages is also affected by the charge of the particles [78]. Particles bearing cationic or anionic surface charges are phagocytized to a higher extent than are neutral particles of the same size and they also present a higher uptake in non-phagocytic cells [79]. According to electrophoretic mobility results, EP nanoparticles had strong negative charges as a result of the phospholipid molecule composition and this anionic charge may further contribute to the higher uptake of this nanosystem by macrophages. When the concentration or poloxamer increases on the surface, the charge is reduced, as is protein adsorption and uptake by cells.

Under serum-free conditions, activated U937 cells behave similarly to A549 (see Fig. 3 of Ref. [46]). When the four lipid nanocapsule systems were exposed to these cells under serum-free conditions, nanoparticle uptake was higher in all cases, and, moreover, cellular damage was observed in the case of EP nanocapsules (the uptake of these samples could not be determined). Once again, when comparing results for the different nanosystems, also in the macrophages, the uptake was reduced when poloxamer was present in the shell in a higher content.

3. Experimental section

3.1. Materials

Poloxamer 407 (Pluronic F127), purchased from Sigma–Aldrich (Spain), is a triblock copolymer based on poly (ethylene oxide)-block - poly (propylene oxide)-block - poly (ethylene oxide) structure, expressed as PEOa–PPOb–PEOa being a = 100 and b = 65. The central hydrophobic block of PPO faces the oil phase while the two hydrophilic chains of PEO remain in the aqueous environment. Coumarin 6, sulforhodamine-B, phorbol myristate, acetate, and olive oil were also purchased from Sigma, and all were used as received except the olive oil, which was previously purified with activated magnesium silicate (Florisil, Fluka) to eliminate free fatty acids. Epikuron 145V, which is a highly purified deoiled phosphatidylcholine-enriched fraction of soybean lecithin, with an average molecular weight of 760 Da, was kindly supplied by Cargill Ibérica S. L. Docetaxel, with a purity ≥97.0%, was obtained from Fluka (Spain). Water was purified in a Milli-Q Academic Millipore system. Other solvents and chemicals used were of the highest grade commercially available.

3.2. Preparation of lipid nanoparticles

The nanosystems studied were prepared by a modified solvent-displacement technique following the procedure of Calvo et al. [80]. Briefly, an organic phase composed of 125 μL of olive oil, dissolved in 0.5 mL of ethanol, and 9.5 mL of acetone, was added to 20 mL of an aqueous phase under magnetic stirring. Epikuron 145V and Pluronic F127 were dissolved in the organic phase and the aqueous phase, respectively, in different combinations. Organic solvents (acetone and ethanol) plus a portion of the volume of water were evaporated in a rotary evaporator at 40 °C, giving a final volume of 18 mL. Finally, nanoparticles were extensively cleaned by dialysis against ultrapure water for 24 h to remove the unbound surfactant molecules.

The hydrophobic core of all the nanosystems were composed by olive oil and, depending on the composition of the organic and aqueous phases, the final sample showed different interface properties, where four different systems were formulated: nanocapsules with a surface shell composed exclusively by Epikuron 145V (referred to as EP); nanocapsules with only Pluronic F127 (PL); and two systems combining both surfactants in different proportion, namely nanocapsules with a predominance of Pluronic F127 (MP) and nanocapsules with a predominance of Epikuron 145V (ME) (Table 3 and Fig. 1).

Docetaxel-loaded lipid nanocapsules were formulated in the same way by dissolving docetaxel in the olive oil phase at a concentration of 0.1% (w/w). The concentration of docetaxel encapsulated in the particles, after different dialysis times, was determined after dissolving an aliquot of docetaxel-loaded nanoparticles with acetonitrile. This sample was centrifuged for 20 min at 4000 × g and the supernatant was measured in the Scientific Instrumentation Center of the University of Granada (Spain), using a SHIMADZU LC-20AC chromatograph with SPD-M20A diode array detector and a C8 Nova-Pak Cartridge column (4 microns, 4.6 × 150 mm); detection was performed at a wavelength of 230 nm. Coumarin 6 lipid nanocapsules were formulated as explained above, dissolving the dye in the olive oil phase at a concentration of 0.025% (w/w).

3.3. Physico-chemical characterization

3.3.1. Size and electrophoretic mobility

The hydrodynamic mean diameter of the nanocapsules and the electrophoretic mobility (με) as a function of pH was determined using a nano-zeta dynamic light-scattering analyzer (Zeta-Sizer NanoZ, Malvern Instruments, UK).

The size and the homogeneity of the size distribution, expressed as polydispersity index (PDI), were calculated by means of the

Table 3
Concentration (mg/mL) of surfactant added in the synthesis of PL, EP, MP and ME nanocapsules.

	Pluronic F127	Epikuron 145V
EP	0	2.22
ME	0.39	2.22
MP	3.89	0.22
PL	3.89	0

Stokes–Einstein equation using the diffusion coefficient measured by dynamic light scattering. The light scattered by the samples was detected at 173°, and the temperature was set at 25 °C. Polydispersity index (PDI) represents the relative variance in the particle size distribution, as further described in the Malvern Zetasizer instrument manual. In general, a sample with a PDI value under 0.2 can be considered as monodisperse.

Electrophoretic mobility was measured after pouring a small volume of the nanocapsule stock (with a total surface area equal to 0.05 m^2) into 1 mL of a low salinity solution (0.002 M) containing the desired buffer. After a 5-min wait for the stabilization of the particle charge in the new pH value, the mobility datum was recorded in triplicate.

3.3.2. Colloidal stability

The colloidal stability experiments provided information related to the charge density of the nanoparticle surface and to the character of the surface hydrophilicity. Sample stability was studied at physiological pH (7.4), monitoring the turbidity of the systems with a Beckman DU 7400 spectrophotometer (working at $\lambda = 570$ nm) while they were forced to coagulate by salinity. NaCl and $CaCl_2$ were used independently as aggregating salts.

From the analysis of aggregation kinetics results, we calculated the critical coagulation concentration (CCC), defined as the minimum salt concentration needed for the most rapid aggregation, and the critical stabilization concentration (CSC) defined as the minimum salt concentration at which the system begins to re-stabilize when salinity is increased even more and related to the surface hydrophilicity [13].

3.3.3. Isothermal titration calorimetry

ITC experiments were conducted using a high-precision ITC-200 titration calorimeter (Microcal Inc., Northampton, MA, USA). The samples were extensively dialyzed against 2 mM sodium phosphate buffer, pH 7.4, using 14,000 MWCO dialysis membranes for nanocapsules and BSA, and 1000 MWCO membranes for FBS. Nanocapsule samples were placed in the cells and were progressively titrated with BSA or FBS. In all cases, a profile of injection volumes from 0.8 to 4 μl was used to better define the BSA and FBS titration curves. The heat that developed after each BSA or FBS injection was determined from the integral of the calorimetric signal. The heat associated with the protein binding process was calculated as the difference between the heat of the reaction and the corresponding heat of protein dilution, as determined from independent titrations of BSA and FBS into the buffer.

The resulting binding isotherms were analyzed by non-linear least-squares fitting to a model corresponding to a single set of identical sites, according to the equation:

$$Q = \frac{V_0 \Delta H}{2K_a}\left[1 + K_a[L_t] + nK_a[M_t] + \sqrt{(1 + K_a[L_t] + nK_a[M_t])^2 - 4nK_a^2[M_t][L_t]}\right] \quad (1)$$

where Q is the net heat of binding, n is the number of binding sites, ΔH is the change in the enthalpy due to the binding process, Ka is the association constant, V_0 is the active cell volume, and $[M_t]$ and $[L_t]$ represent the total concentrations of nanocapsule and the titrant, respectively.

The binding isotherms corresponding to the titration of EP and ME nanocapsules with FBS, which were not able to be properly reproduced by this model, were analyzed according to a model of two sets of independent binding sites. According to this model, the net heat of binding can be expressed as:

$$Q = V_0[M_t]\left[\Delta H_1 \frac{n_1 K_1[L_t]}{1 + K_1[L_t]} + \Delta H_2 \frac{n_2 K_2[L_t]}{1 + K_2[L_t]}\right] \quad (2)$$

where Q is the net heat of binding, n_1 and n_2 are the number of sites of each class, ΔH1 and ΔH_2 are the change in the enthalpy due to the binding process for each site, K_1 and K_2 are the association constants for each site, V_0 is the active cell volume, and $[M_t]$ and $[L_t]$ are the total concentrations of nanocapsule and the titrant, respectively. In this case, the molar concentration of FBS was estimated considering a total protein concentration in FBS of 40 mg/mL and the molecular weight of BSA.

In all cases, the models were implemented in Origin 7.0 software (OriginLab Corporation, Northampton, MA, USA). For the least-squares fit, the number of binding sites, the association constant, and the binding enthalpy were considered to be floating parameters.

3.4. Cell lines and culture conditions

The human lung-cancer cell line A549, supplied by the Scientific Instrumentation Center of the University of Granada (Spain), was maintained as monolayer cultures in DMEM (Sigma) and the human leukemic monocytic lymphoma cell line, U937, was maintained in a monocytic cell suspension in RPMI-1640 (Sigma) culture medium. Both cell lines were supplemented with heat-inactivated 10% (v/v) fetal bovine serum (FBS, Sigma), 2% L-glutamine, 2.7% sodium bicarbonate, 1% Hepes buffer, and 1% of penicillin/streptomycin solution in a humidified atmosphere of 5% CO_2 at 37 °C. Treatment of U937 cells with phorbol 12-myristate 13-acetate (PMA) mimics the activation/differentiation of monocytes *in vivo* [81]. Cells were activated to macrophages for 48 h with the addition of 10 ng/mL PMA to the culture medium [82].

3.5. Uptake studies of coumarin 6-loaded nanocapsules

U937 cells ($1{,}5 \times 10^5$), previously activated with PMA for 48 h, and A549 cells ($1{,}5 \times 10^5$) were seeded into 6-well plates in cDMEM. After 24 h, before exposure to nanoparticles, the cDMEM was removed; then cells were washed once with PBS buffer prior to the addition of the nanoparticle dispersions. Coumarin 6-loaded nanocapsule dispersions were prepared by diluting the nanoparticle stock to the required concentration in SF or cDMEM just before addition to cells. In the control groups, cells were treated with non-fluorescent nanocarriers. After cell incubation, cells were washed three times with PBS to remove free and adhering nanocapsules [70], then harvested using phosphate-buffered saline-ethylenediamine-tetraacetic acid (PBS-EDTA) and pelleted by centrifugation. Then, the cells were fixed at room temperature with a 4% formalin solution for 20 min and re-suspended in PBS before measuring the cell-associated fluorescence (15,000 cells per sample) using a FacsCalibur flow cytometry device (Becton Dickinson). The results are represented by averaging the distribution of cell fluorescence intensity, working with three independent replicates. Error bars represent the standard deviation between replicates. Each experiment was performed at least three times.

In addition, uptake efficiency in cDMEM of Coumarin 6-loaded nanoparticles in the A549 cell line was qualitatively studied by fluorescence microscopy. Cells were imaged by a Leica DM5500 microscope. All experiments were performed in triplicate and replicated at least twice.

3.6. Cytotoxicity assay

A549 cells (2×10^4) were plated into 24-well plates under the

culture conditions detailed above. Cells were fed with fresh cDMEM and increased concentrations of free and encapsulated docetaxel for 48 h. Then cells were counted using the sulforhodamine-B (SRB) colorimetric assay in a Titertek Multiscan apparatus (Flow, Irvine, CA, USA) at 492 nm. IC_{50} values were calculated from semi-logarithmic dose–response curves by linear fitting. All experiments were performed at least three times in triplicate wells.

3.7. Statistical analysis

SPSS 7.5 software (IBM, Chicago, IL, USA) was used for all data analyses. Results were compared with Student's t test. All data were expressed as means ± standard deviation (SD). Differences were considered statistically significant at a P value of <0.05.

4. Conclusions

In this study, different techniques were used to investigate how the surface composition of lipid nanocapsules influences the protein adsorption and, subsequently, the uptake by cancer cells, therapeutic efficacy, and uptake by macrophages. ITC and electrophoresis were used to characterize the interactions between proteins and the different nanoparticle surfaces, showing that the presence of poloxamer, a non-ionic surfactant, on the surface of lipid nanocapsules significantly reduced the protein adsorption when particles were dispersed in culture medium with proteins. Interestingly, ITC in full serum showed two different binding events, characterized by dissociation constants in the micromolar and nanomolar range, probably due to the presence of a soft and hard corona, respectively, on the nanoparticles. The formulation containing high amount of poloxamer however showed only binding with a dissociation constant in the micromolar range, indicating that addition of this polymer prevents formation of hard corona, thus could protect the nanocapsules from unspecific binding.

At the same time, increasing the density of the poloxamer also masked interactions with cells thus lowered uptake by cancer cells and consecutively their therapeutic efficacy. Similarly, macrophage association was also significantly reduced, thus suggesting that addition of poloxamer protects the capsules from clearance and could increase blood circulation time. When exposed to cells in serum free conditions, the accumulation of all lipid nanocapsules in both cell lines proved higher than what observed in complete medium, indicating that the nature of interactions of the same material in the presence or absence of proteins was different. Hence, the nature and concentration of the surfactant can be used to control the interactions of lipid nanocapsules with biological environment, which can be useful for *in vivo* anticancer assays of these nanocapsules. Addition of a coating like PL which reduces strongly unspecific binding leads to a lower uptake by macrophages, thus could help increase blood circulation time, but at the same time can also lower uptake into the target cells, thus lowering therapeutic efficacy. Thus, ideal formulations should be designed to balance these two opposing effects. Addition of targeting moieties, which can be easily conjugated on the shell of these nanocapsules [12,13] might help to increase recognition and uptake at the target sites.

Overall, the approaches presented here help to understand the effect of each component on the final efficacy of drug formulations, thus guiding the design of successful nanomedicines. Lipid nanocapsules confirm to be a versatile platform that can be easily engineered to achieve the desired properties for specific applications.

Acknowledgments

The authors gratefully acknowledge Dr. Mattia Bramini for insightful discussions and technical support with confocal microscopy and Dr. Gustavo Ortiz Ferrón for assistance with flow cytometer. This work was supported by the projects MAT2010-20370 and MAT2013-43922-R (European FEDER support included, MICINN, Spain), PI10/02295 (Instituto de Salud Carlos III, Fondo de Investigación Sanitaria, FEDER funds) and P07-FQM2496, P10-CTS-6270 and P07-FQM3099 (Junta de Andalucía, Spain).

Appendix A. Supplementary data

Supplementary data related to this article can be found at http://dx.doi.org/10.1016/j.biomaterials.2015.04.049.

References

[1] M. Ferrari, Nat. Rev. Cancer 5 (2005) 161–171.
[2] I. Ojea-Jimenez, L. Garcia-Fernandez, J. Lorenzo, V.F. Puntes, Acs Nano 6 (2012) 7692–7702.
[3] Z.Y. Xiao, E. Levy-Nissenbaum, F. Alexis, A. Luptak, B.A. Teply, J.M. Chan, J.J. Shi, E. Digga, J. Cheng, R. Langer, O.C. Farokhzad, Acs Nano 6 (2012) 696–704.
[4] T.G. Mason, J.N. Wilking, K. Meleson, C.B. Chang, S.M. Graves, J. Phys.-Condens. Matter 18 (2006) R635–R666.
[5] N.T. Huynh, C. Passirani, P. Saulnier, J.P. Benoit, Int. J. Pharm. 379 (2009) 201–209.
[6] S. Ramishetti, L. Huang, Ther. Deliv. 3 (2012) 1429–1445.
[7] P. Sanchez-Moreno, H. Boulaiz, J.L. Ortega-Vinuesa, J.M. Peula-Garcia, A. Aranega, Int. J. Mol. Sci. 13 (2012) 4906–4919.
[8] M.N. Khalid, P. Simard, D. Hoarau, A. Dragomir, J.C. Leroux, Pharm. Res. 23 (2006) 752–758.
[9] M.V. Lozano, D. Torrecilla, D. Torres, A. Vidal, F. Dominguez, M.J. Alonso, Biomacromolecules 9 (2008) 2186–2193.
[10] H. Maeda, Adv. Enzyme Regul. 41 (2001) 189–207.
[11] D. Torrecilla, M.V. Lozano, E. Lallana, J.I. Neissa, R. Novoa-Carballal, A. Vidal, E. Fernandez-Megia, D. Torres, R. Riguera, M.J. Alonso, F. Dominguez, Eur. J. Pharm. Biopharm. 83 (2013) 330–337.
[12] A. Rata-Aguilar, P. Sanchez-Moreno, A.B. Jodar-Reyes, A. Martin-Rodriguez, H. Boulaiz, J.A. Marchal-Corrales, J.M. Peula-Garcia, J.L. Ortega-Vinuesa, J. Bioact. Compat. Polym. 27 (2012) 388–404.
[13] P. Sanchez-Moreno, J.L. Ortega-Vinuesa, H. Boulaiz, J.A. Marchal, J.M. Peula-Garcia, Biomacromolecules 14 (2013) 4248–4259.
[14] S. Tenzer, D. Docter, J. Kuharev, A. Musyanovych, V. Fetz, R. Hecht, F. Schlenk, D. Fischer, K. Kiouptsi, C. Reinhardt, K. Landfester, H. Schild, M. Maskos, S.K. Knauer, R.H. Stauber, Nat. Nanotechnol. 8 (2013) 772–U1000.
[15] M.P. Monopoli, C. Aberg, A. Salvati, K.A. Dawson, Nat. Nanotechnol. 7 (2012) 779–786.
[16] A.E. Nel, L. Madler, D. Velegol, T. Xia, E.M.V. Hoek, P. Somasundaran, F. Klaessig, V. Castranova, M. Thompson, Nat. Mater. 8 (2009) 543–557.
[17] C. Rocker, M. Potzl, F. Zhang, W.J. Parak, G.U. Nienhaus, Nat. Nanotechnol. 4 (2009) 577–580.
[18] H. de Puig, S. Federici, S.H. Baxamusa, P. Bergese, K. Hamad-Schifferli, Small 7 (2011) 2477–2484.
[19] U. Sakulkhu, L. Maurizi, M. Mahmoudi, M. Motazacker, M. Vries, A. Gramoun, M.G.O. Beuzelin, J.P. Vallee, F. Rezaee, H. Hofmann, Nanoscale 6 (2014) 11439–11450.
[20] A. Salvati, A.S. Pitek, M.P. Monopoli, K. Prapainop, F.B. Bombelli, D.R. Hristov, P.M. Kelly, C. Aberg, E. Mahon, K.A. Dawson, Nat. Nanotechnol. 8 (2013) 137–143.
[21] S. Hak, E. Helgesen, H.H. Hektoen, E.M. Huuse, P.A. Jarzyna, W.J.M. Mulder, O. Haraldseth, C.D. Davies, Acs Nano 6 (2012) 5648–5658.
[22] A. Cifuentes-Rius, H. de Puig, J.C. Kah, S. Borros, K. Hamad-Schifferli, ACS Nano 7 (2013) 10066–10074.
[23] C. Fang, N. Bhattarai, C. Sun, M.Q. Zhang, Small 5 (2009) 1637–1641.
[24] X.Q. Shan, C.S. Liu, Y. Yuan, F. Xu, X.Y. Tao, Y. Sheng, H.J. Zhou, Colloids Surf. B-Biointerf. 72 (2009) 303–311.
[25] L.G. Delogu, A. Magrini, A. Bergamaschi, N. Rosato, M.I. Dawson, N. Bottini, M. Bottini, Bioconjug. Chem. 20 (2009) 427–431.
[26] C.D. Walkey, J.B. Olsen, H.B. Guo, A. Emili, W.C.W. Chan, J. Am. Chem. Soc. 134 (2012) 2139–2147.
[27] R.H. Muller, K.H. Wallis, Int. J. Pharm. 89 (1993) 25–31.
[28] R.H. Muller, S. Maassen, H. Weyhers, W. Mehnert, J. Drug Target. 4 (1996) 161–170.
[29] T.M. Goppert, R.H. Muller, J. Drug Target. 11 (2003) 225–231.
[30] U. Gaur, S.K. Sahoo, T.K. De, P.C. Ghosh, A. Maitra, P.K. Ghosh, Int. J. Pharm. 202 (2000) 1–10.
[31] S.M. Moghimi, A.C. Hunter, Trends Biotechnol. 18 (2000) 412–420.
[32] W. Hong, D. Chen, X. Zhang, J. Zeng, H. Hu, X. Zhao, M. Qiao, Biomaterials 34

(2013) 9602–9614.
[33] V. Saxena, M.D. Hussain, J. Biomed. Nanotechnol. 9 (2013) 1146–1154.
[34] W. Zhang, Y.A. Shi, Y.Z. Chen, J.A. Ye, X.Y. Sha, X.L. Fang, Biomaterials 32 (2011) 2894–2906.
[35] Y.Z. Wang, J.G. Hao, Y.J. Li, Z.W. Zhang, X.Y. She, L.M. Han, X.L. Fang, Biomaterials 33 (2012) 4741–4751.
[36] A. Torcello-Gómez, M. Wulff-Pérez, M. Gálvez-Ruiz, A. Martín-Rodríguez, M. Cabrerizo Vílchez, M.-V. J, Adv. Colloid Interfac. 206 (2014) 414–427.
[37] S.M. Moghimi, A.C. Hunter, J.C. Murray, Pharmacol. Rev. 53 (2001) 283–318.
[38] S. Lindman, I. Lynch, E. Thulin, H. Nilsson, K.A. Dawson, S. Linse, Nano Lett. 7 (2007) 914–920.
[39] G. Baier, C. Costa, A. Zeller, D. Baumann, C. Sayer, P.H.H. Araujo, V. Mailander, A. Musyanovych, K. Landfester, Macromol. Biosci. 11 (2011) 628–638.
[40] R. Huang, R.P. Carney, K. Ikuma, F. Stellacci, B.L. Lau, ACS Nano 8 (2014) 5402–5412.
[41] S. Winzen, S. Schoettler, G. Baier, C. Rosenauer, V. Mailaender, K. Landfestera, K. Mohr, Nanoscale 7 (2015) 2992.
[42] F. Alexis, E. Pridgen, L.K. Molnar, O.C. Farokhzad, Mol. Pharm. 5 (2008) 505–515.
[43] M.J. Santander-Ortega, M.V. Lozano-Lopez, D. Bastos-Gonzalez, J.M. Peula-Garcia, J.L. Ortega-Vinuesa, Colloid Polym. Sci. 288 (2010) 159–172.
[44] A.K. Gupta, A.S. Curtis, Biomaterials 25 (2004) 3029–3040.
[45] P. Couvreur, G. Barratt, E. Fattal, P. Legrand, C. Vauthier, Crit. Rev. Ther. Drug Carr. Syst. 19 (2002) 99–134.
[46] P. Sánchez-Moreno, J.L. Ortega-Vinuesa, H. Boulaiz, J.A. Marchal-Corrales, J.M. Peula-García, Data Brief (2015) (Submitted for publication).
[47] M.J. Santander-Ortega, A.B. Jodar-Reyes, N. Csaba, D. Bastos-Gonzalez, J.L. Ortega-Vinuesa, J. Colloid Interface Sci. 302 (2006) 522–529.
[48] A. Torcello-Gomez, M.J. Santander-Ortega, J.M. Peula-Garcia, J. Maldonado-Valderrama, M.J. Galvez-Ruiz, J.L. Ortega-Vinuesa, A. Martin-Rodriguez, Soft Matter 7 (2011) 8450–8461.
[49] R. Gref, M. Luck, P. Quellec, M. Marchand, E. Dellacherie, S. Harnisch, T. Blunk, R.H. Muller, Colloids Surf. B Biointerf. 18 (2000) 301–313.
[50] I. Lynch, K.A. Dawson, Nano Today 3 (2008) 40–47.
[51] J.M. Peula, R. HidalgoAlvarez, R. Santos, J. Forcada, F.J. DelasNieves, J. Mater. Sci.-Mater. M. 6 (1995) 779–785.
[52] J.L.O. Vinuesa, M.J.G. Ruiz, R. HidalgoAlvarez, Langmuir 12 (1996) 3211–3220.
[53] F. Alexis, E. Pridgen, L.K. Molnar, O.C. Farokhzad, Mol. Pharm. 5 (2008) 505–515.
[54] P.P. Karmali, D. Simberg, Expert Opin. Drug Deliv. 8 (2011) 343–357.
[55] M. Roser, D. Fischer, T. Kissel, Eur. J. Pharm. Biopharm. 46 (1998) 255–263.
[56] J.A. Molina-Bolivar, J.L. Ortega-Vinuesa, Langmuir 15 (1999) 2644–2653.
[57] J.A. Molina-Bolivar, F. Galisteo-Gonzalez, R. Hidalgo-Alvarez, J. Immunol. Methods 211 (1998) 87–95.
[58] E. Caballero-Diaz, C. Pfeiffer, L. Kastl, P. Rivera-Gil, B. Simonet, M. Valcarcel, J. Jimenez-Lamana, F. Laborda, W.J. Parak, Part Part Syst. Char. 30 (2013) 1079–1085.
[59] P. Sanchez-Moreno, J.L. Ortega-Vinuesa, A. Martin-Rodriguez, H. Boulaiz, J.A. Marchal-Corrales, J.M. Peula-Garcia, Int. J. Mol. Sci. 13 (2012) 2405–2424.
[60] T. Cedervall, I. Lynch, S. Lindman, T. Berggard, E. Thulin, H. Nilsson, K.A. Dawson, S. Linse, P Natl. Acad. Sci. U.S.A. 104 (2007) 2050–2055.
[61] M.P. Monopoli, D. Walczyk, A. Campbell, G. Elia, I. Lynch, F.B. Bombelli, K.A. Dawson, J. Am. Chem. Soc. 133 (2011) 2525–2534.
[62] A. Gessner, A. Lieske, B.R. Paulke, R.H. Muller, J. Biomed. Mater. Res. A 65A (2003) 319–326.
[63] T. Cedervall, I. Lynch, M. Foy, T. Berggad, S.C. Donnelly, G. Cagney, S. Linse, K.A. Dawson, Angew. Chem. Int. Ed. 46 (2007) 5754–5756.
[64] L. Treuel, S. Brandholt, P. Maffre, S. Wiegele, L. Shang, G.U. Nienhaus, Acs Nano 8 (2014) 503–513.
[65] I. Rivolta, A. Panariti, B. Lettiero, S. Sesana, P. Gasco, M.R. Gasco, M. Masserini, G. Miserocchi, J. Physiol. Pharmacol. 62 (2011) 45–53.
[66] Y.T. Liu, K. Li, J. Pan, B. Liu, S.S. Feng, Biomaterials 31 (2010) 330–338.
[67] P.F. Xu, Q. Yin, J.N. Shen, L.L. Chen, H.J. Yu, Z.W. Zhang, Y.P. Li, Int. J. Pharm. 454 (2013) 21–30.
[68] A. Salvati, C. Aberg, T. dos Santos, J. Varela, P. Pinto, I. Lynch, K.A. Dawson, Nanomed.-Nanotechnol. 7 (2011) 818–826.
[69] A. Lesniak, A. Salvati, M.J. Santos-Martinez, M.W. Radomski, K.A. Dawson, C. Aberg, J. Am. Chem. Soc. 135 (2013) 1438–1444.
[70] T. dos Santos, J. Varela, I. Lynch, A. Salvati, K.A. Dawson, Small 7 (2011) 3341–3349.
[71] A. Lesniak, F. Fenaroli, M.R. Monopoli, C. Aberg, K.A. Dawson, A. Salvati, Acs Nano 6 (2012) 5845–5857.
[72] A. Lesniak, A. Salvati, M.J. Santos-Martinez, M.W. Radomski, K.A. Dawson, C. Aberg, J. Am. Chem. Soc. 135 (2013) 1438–1444.
[73] C. Montis, D. Maiolo, I. Alessandri, P. Bergese, D. Berti, Nanoscale 6 (2014) 6452–6457.
[74] B.R. Liu, M. Yang, R.T. Li, Y.T. Ding, X.P. Qian, L.X. Yu, X.Q. Jiang, Eur. J. Pharm. Biopharm. 69 (2008) 527–534.
[75] G. Storm, S.O. Belliot, T. Daemen, D.D. Lasic, Adv. Drug Deliv. Rev. 17 (1995) 31–48.
[76] D.E. Owens, N.A. Peppas, Int. J. Pharm. 307 (2006) 93–102.
[77] S. Stolnik, B. Daudali, A. Arien, J. Whetstone, C.R. Heald, M.C. Garnett, S.S. Davis, L. Illum, Biochimica Biophysica Acta-Biomembranes 1514 (2001) 261–279.
[78] L. Thiele, H.P. Merkle, E. Walter, Pharm. Res. 20 (2003) 221–228.
[79] E. Frohlich, Int. J. Nanomed. 7 (2012) 5577–5591.
[80] P. Calvo, C. RemunanLopez, J.L. VilaJato, M.J. Alonso, Colloid Polym. Sci. 275 (1997) 46–53.
[81] J.O. Minta, L. Pambrun, Am. J. Pathol. 119 (1985) 111–126.
[82] M.Y. Liu, M.C. Wu, Exp. Hematol. 20 (1992) 974–979.